International Journal of Engineering, Mathematical and Physical Sciences
ISSN: 2517-9934
Vol:8, No:7, 2014

Grid Independence Study of Flow Past a Square Cylinder Using the Multi-Relaxation-Time Lattice Boltzmann Method

Shams-Ul-Islam, Hamid Rahman, Waqas Sarwar Abbasi

Abstract**—**Numerical calculations of flow around a square cylinder are presented using the multi-relaxation-time lattice Boltzmann method at Reynolds number 150. The effects of upstream locations, downstream locations and blockage are investigated systematically. A detail analysis are given in terms of time-trace analysis of drag and lift coefficients, power spectra analysis of lift coefficient, vorticity contours visualizations and phase diagrams. A number of physical quantities mean drag coefficient, drag coefficient, Strouhal number and root-mean-square values of drag and lift coefficients are calculated and compared with the well resolved experimental data and numerical results available in open literature. The results had shown that the upstream, downstream and height of the computational domain are at least 7.5, 37.5 and 12 diameters of the cylinder, respectively.

Keywords**—**Grid independence, Multi-relaxation-time lattice Boltzmann method, Physical quantities, Square cylinder, Vorticity contours visualizations.

I. Introduction

PREDICTING the flow field around a square cylinder is the main issue of recent research due to development of new numerical methods and advancement of hardwares. Many similar investigations recently have been made, but the numerical results always show some small discrepancies even the global trends are similar. One of the main reasons for such discrepancies is the difference of the grid points during the construction. In this paper, we carry out a two-dimensional numerical study of flow around a square cylinder at low Reynolds number at different combinations of computational domain. The main reason for chosen square cylinder is that this geometry is relatively easy to simulate on a cartesian grid using the modest computing resources. In this study we will use the multi-relaxation-time lattice Boltzmann method.

The flow around a square cylinder has been studied experimentally [1], [2] and numerically [3]-[6] amongst others. These studies document the dependence of the drag coefficient and Strouhal number on the blockage ratio and Reynolds number. Suzuki et al. [7] numerically examined the weak dependence of Strouhal number on the incoming velocity profile. Sohankar et al. [3] numerically examined the influence of the upstream, downstream and side wall locations using the incompressible SIMPLEC finite volume code at low Reynolds numbers ranging from 45 to 250. They observed that the effect of the computational domain almost becomes negligible when the upstream location is about 11.1*d* (where *d* is the size of the cylinder), downstream location is about 30*d* and distance between the walls (blockage) is about 5*d*. Sohankar et al. [8] numerically examined the effect of blockage and outlet boundary conditions on flow past a square cylinder using an incompressible SIMPLEC code with a non-staggered grid arrangement. They also compared the sommerfield boundary condition with the Neumann boundary condition and observed that if downstream location is approximately larger than 25*d*, then the influence of the Neumann boundary condition is effectively damped out. They also investigated that when the blockage decrease from 5% to 2.5%, the Strouhal number, mean drag coefficient and root-mean-square value of the lift coefficient decreasing 1.5%. Ali et al. [9] numerically studied the grid convergence for flow past a square cylinder at a low Reynolds number using the Direct Numerical Simulation (DNS) method. They investigated different grid refinements using different boundary conditions and observed the influence of grid points on the flow past a square cylinder. Ying et al. [10] numerically studied the three-dimensional flow around rectangular cylinders at Reynolds number of 21400 using the ANSYS FLUENT for different blockages. Doolan [11] examined the three different grid resolutions using the DNS method around a square cylinder and found that when the blockage is 0.0167 the solution converged. An important goal of this study is to provide a comprehensive analysis of computational domain with all possible informations for flow around a square cylinder in terms of physical quantities, vorticity contour.

The rest of the paper is organized as follows: A brief overview of the multi-relaxation-time lattice Boltzmann method is given in Section II, initial and boundary conditions and important physical parameters are presented in Sections III and IV. The problem description is presented in Section V. The effects of the computational domain on the physical quantities, vortex shedding frequencies and the flow structures are discussed in Section VI compared with experimental data and numerical results. Finally important findings are summarized in Section VII.

Shams-Ul-Islam is with the Mathematics Department, COMSATS Institute of Information Technology Islamabad, 44000, Pakistan (corresponding author, Phone: 0092-3139840066; e-mail: islam_shams@comsats.edu.pk).

Hamid Rahman and Waqas Sarwar Abbasi are with the Mathematics Department, COMSATS Institute of Information Technology Islamabad, 44000, Pakistan (e-mail: hamid_icp@yahoo.com, waqas-555@hotmail.com).

II. Multi-Relaxation-Time Lattice Boltzmann Method

The lattice Boltzmann equation (LBE) is a new numerical scheme originated from the lattice gas model (LGM) in order to overcome the main difficulties in LGM [12]. In LBE, a group of microscopic particles discretized the fluid field. The density distribution function of these particles performs two different kinds of motions: collision and streaming. In this paper, we use the $D2Q9$ model (where D is the space dimensions and Q is the number of particles at a computational node) on a square lattice with lattice spacing $\delta x = \delta y$ (Fig. 1). Each computational node comprises three different kinds of particles, rest particles, particles that move along the coordinate directions, and moving particles along diagonal directions.

The lattice Bhatnagar-Gross-Krook (BGK) equation is the simplest LBE, based on single-relaxation-time (SRT) approximation [13]. Nowadays the most popular lattice Boltzmann model is the lattice BGK equation due to its simplicity. However, the numerical instability [14] and inaccuracy in boundary conditions during implementation [15] are some issues of this model. The multi-relaxation-time (MRT) model introduced by d'Hmmieres [16] overcomes these deficiencies in the BGK models. The MRT collision operators have advantages over BGK [13] and [14]. For example, fixed Prandtl number ($Pr = 1$) and fixed ratio between the kinematic and bulk viscosities overcomes these defects of BGK model. In case of MRT-LBM, the different relaxation times can be adjusted individually to achieve 'optimal' stability [14].

In MRT-LBM with nine velocities, $f_i(r_j, t_n)$, $i \in \{0, \ldots, 8\}$, is a set of velocity distribution functions, is defined on each lattice node r_j and for time t_n. The evolution equation for the MRT-LBM is given below

$$f\left(\boldsymbol{r}_j + e_i \delta t, t_n + \delta t\right) = f\left(\boldsymbol{r}_j, t_n\right) - \boldsymbol{M}^{-1} S\left(\boldsymbol{m}\left(\boldsymbol{r}_j, t_n\right) - \boldsymbol{m}^{eq}\left(\boldsymbol{r}_j, t_n\right)\right) \tag{1}$$

where $f(\boldsymbol{r}_j, t_n)$, $\boldsymbol{m}(\boldsymbol{r}_j, t_n)$, and $\boldsymbol{m}^{\mathrm{eq}}(\boldsymbol{r}_j, t_n)$ are nine-dimensional distribution functions vectors, the moments, and the equilibria of moments, respectively, such as $\boldsymbol{f} = (f_0, f_1, \ldots, f_8)^{\mathrm{T}}$, T is the transpose operator, and $\boldsymbol{m} = (m_0, m_1, \ldots, m_8)^{\mathrm{T}}$. S is the relaxation matrix in the moment space and $\boldsymbol{M}$ is the transformation matrix such that $\boldsymbol{m} = \boldsymbol{M}\boldsymbol{f}$ and $\boldsymbol{f} = \boldsymbol{M}^{-1}\boldsymbol{m}$. $\boldsymbol{e}_i$ ($\boldsymbol{e}_0 = (0, 0)$ for $i = 0$, $\boldsymbol{e}_i = (\pm 1, 0)$ for $i = 1, 3$ and $\boldsymbol{e}_i = (0, \pm 1)$ for $i = 2, 4$ and $\boldsymbol{e}_i = (\pm 1, \pm 1)$ for $i = 5, 6, 7, 8$) is a set of nine discrete velocity in $D2Q9$ model and δ_t is the time step. In this paper the lattice grid spacing and time step is equal to one.

The matrices M and S of the incompressible lattice Boltzmann method are given below:

$$\boldsymbol{M} = \begin{bmatrix} 1 & 1 & 1 & 1 & 1 & 1 & 1 & 1 & 1 \\ -4 & -1 & -1 & -1 & -1 & 2 & 2 & 2 & 2 \\ 4 & -2 & -2 & -2 & -2 & 1 & 1 & 1 & 1 \\ 0 & 1 & 0 & -1 & 0 & 1 & -1 & -1 & 1 \\ 0 & -2 & 0 & 2 & 0 & 1 & -1 & -1 & 1 \\ 0 & 0 & 1 & 0 & -1 & 1 & 1 & -1 & -1 \\ 0 & 0 & -2 & 0 & 2 & 1 & 1 & -1 & -1 \\ 0 & 1 & -1 & 1 & -1 & 0 & 0 & 0 & 0 \\ 0 & 0 & 0 & 0 & 0 & 1 & -1 & 1 & -1 \end{bmatrix} \tag{2}$$

and

$$s = \mathrm{diag}\left(0, S_1, S_2, 0, S_3, 0, S_6, S_7, S_8\right) \tag{3}$$

The moment vector $\boldsymbol{m}$ in MRT-LBM are arranged in the following order: $m_0 = \rho$, $m_1 = e$, $m_2 = \varepsilon$, $m_{3,5} = j_{x,y}$, $\boldsymbol{J} = (j_x, j_y)$, $m_{4,6} = q_{x,y}$, and $m_{7,8} = p_{xx,xy}$ are the fluid density, energy, energy square, components of the momentum, components of the energy, components of the symmetric and traceless strain rate tensor, respectively. These nine moments are generally divided into two main groups: (ρ, m_3, m_5) and (m_1, m_2, m_4, m_6, m_7, m_8) are the conserved moments and locally conserved in the collision process and the non-conserved moments. The later one, are calculated from the following relaxation equations:

$$m_j^{*} = m_j^{**} + s_j\left(m_j^{eq} - m_j^{**}\right) \tag{4}$$

where m_j^{*}, m_j^{**}, s_j, and m_j^{eq} are the moment after collision, the moment before collision, the relaxation rates that are the diagonal elements of the matrix S and the corresponding equilibrium moments, respectively. It is important to mention here that s_0, s_3, and s_5 are not relevant collision rates and only related to the conserved moments. The relaxation rates s_7 and s_8 for consistent dynamics viscosity must be equal ($s_7 = s_8$). The other relaxation rates in the range $0 < s_i < 2$ can be freely chosen. The relaxation rates s_7 and s_8 are related to the kinematic viscosity ν by (5):

$$\nu = c_s^2 \delta t\left(\frac{1}{s_7} - 0.5\right) = c_s^2 \delta t\left(\frac{1}{s_8} - 0.5\right) \tag{5}$$

where $c_s = 0.5773$ is the lattice speed of sound in case of unit lattice spacing and time step.

The non-conserved moments $\boldsymbol{m}^{\mathrm{eq}}$ are chosen to be:

$$\begin{aligned} e^{eq} &= -2\rho + 3\left(j_x^2 + j_y^2\right) \\ \varepsilon^{eq} &= \rho - 3\left(j_x^2 + j_y^2\right)\Big/\rho_0 \\ q_x^{eq} &= -j_x \\ q_y^{eq} &= -j_y \\ p_{xx}^{eq} &= \left(j_x^2 - j_y^2\right)\Big/\rho_0 \\ p_{yy}^{eq} &= j_x j_y \Big/ \rho_0 \end{aligned} \tag{6}$$

The constant mean density ρ_0 usually set to be unity in numerical simulations.

From the moments of the distribution functions the macroscopic fluid variables, density ρ, velocity $\boldsymbol{u}$, and pressure P, are calculated as follows:

$$\rho = \sum_{i=0}^{8} f_i \tag{7}$$

$$J\left(j_x, j_y\right) = \rho \boldsymbol{u} = \sum_{i=1}^{8} f_i e_i \tag{8}$$

$$P = \rho c_s^2 \tag{9}$$

where $\boldsymbol{u} = (u, v)$ is the velocity vector.

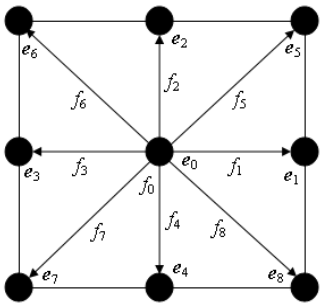

Fig. 1 *D2Q9* lattice structure

One can easily find the application of lattice Boltzmann method using the single-relaxation-time and multi-relaxation-time lattice Boltzmann methods for bluff body flows [17]-[24].

III. Initial and Boundary Conditions

The initial and boundary conditions are discussed in this section. Uniform flow with velocity $U_{\max}$ is incorporated using the equilibrium particle distribution function at the inlet boundary where

$$u = U_{\max} \text{ and } v = 0 \tag{10}$$

In case of parabolic velocity profile we will use the following equation:

$$u = U_{\max}\left(1 - 2\,y/H\right)\left(1 + 2\,y/H\right) \tag{11}$$

where y is the transverse direction and H is the height of the computational domain.

The computational domain behind the cylinders is selected to be large enough so that the flow at the outflow boundary can be considered to be fully developed. Therefore a fixed pressure in terms of the equilibrium distribution function is imposed at the outlet. For such implementation, the velocity components are extrapolated downstream[18]. A no-slip ($u = v = 0$) wall boundary condition is applied to the surfaces of cylinder 25] and at both bottom and top boundaries of the computational domain. The total fluid force on the square cylinders is calculated using the momentum exchange method [26]. In this study we set $s_0 = s_3 = s_5 = 0$, $s_1 = 1.1$, $s_2 = 1.0$ and $s_4 = s_6 = 1.2$.

IV. Important Physical Parameters

The Reynolds number (*Re*) is defined by:

$$Re = U_{\max} d / \nu \tag{12}$$

where d is the size of the cylinder and ν is the kinematic viscosity.

Other important parameters are the Strouhal number (*St*), the drag coefficient (*Cd*), the lift coefficient (*Cl*) and the blockage ratio *B*.

$$St = f_s d / U_{\max} \tag{13}$$

$$Cd = F_d / 0.5\rho U_{\max}^2 d \tag{14}$$

$$Cl = F_l / 0.5\rho U_{\max}^2 d \tag{15}$$

$$B = H/d \tag{16}$$

where f_s is the vortex shedding frequency, F_d and F_l are the force components in the in-line and transverse directions, respectively. All the computations are carried out on a Dawning Parallel Computer TC4000. The root-mean-square value of drag and lift coefficients are calculated using the following two equations:

$$Cdrms = \sqrt{\sum_{t=1}^{n}\left[Cd\left(t\right) - mean(Cd)\right]^2 / n} \tag{17}$$

$$Clrms = \sqrt{\sum_{t=1}^{n}\left[Cl\left(t\right) - mean(Cl)\right]^2 / n} \tag{18}$$

where n is the total number of time steps.

V. Problem Description

The schematic configuration of flow around a square cylinder in a uniform flow is shown in Fig. 1. In Fig. 2, is the size of the cylinder, *Umax* is the maximum uniform inflow velocity at the inlet and H is the height of the computational domain. Furthermore, L_u is the upstream distance, L_d is the downstream distance and L is the length of the channel. The flow is two-dimensional in the longitudinal (x) and transverse (y) directions. The flow velocity components u and v are in the longitudinal and transverse directions, respectively. The selected cases for computation are given in Table I.

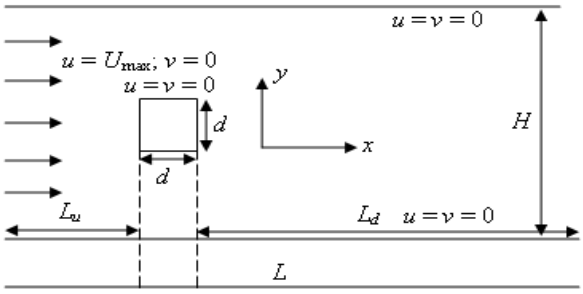

Fig. 2 Schematic configuration of flow past a square cylinder

TABLE I
SELECTED CASES FOR SIMULATION

Cases	$L (= L_u + L_d + d) \times H$
$L_u = 2.5d$; $L_d = 37.5d$; $H = 13d$	821 × 261
$L_u = 4d$; $L_d = 37.5d$; $H = 13d$	851 × 261
$L_u = 5d$; $L_d = 37.5d$; $H = 13d$	871 × 261
$L_u = 6.5d$; $L_d = 37.5d$; $H = 13d$	901 × 261
$L_u = 7.5d$; $L_d = 37.5d$; $H = 13d$	921 × 261
$L_u = 9d$; $L_d = 37.5d$; $H = 13d$	951 × 261
$L_u = 10d$; $L_d = 37.5d$; $H = 13d$	971 × 261
$L_u = 11.5d$; $L_d = 37.5d$; $H = 13d$	1001 × 261
$L_u = 7.5d$; $L_d = 15d$; $H = 13d$	471 × 261
$L_u = 7.5d$; $L_d = 25d$; $H = 13d$	671 × 261
$L_u = 7.5d$; $L_d = 30d$; $H = 13d$	771 × 261
$L_u = 7.5d$; $L_d = 33.5d$; $H = 13d$	841 × 261
$L_u = 7.5d$; $L_d = 37.5d$; $H = 13d$	921 × 261
$L_u = 7.5d$; $L_d = 40d$; $H = 13d$	971 × 261
$L_u = 7.5d$; $L_d = 45d$; $H = 13d$	1071 × 261
$L_u = 7.5d$; $L_d = 50d$; $H = 13d$	1171 × 261
$L_u = 7.5d$; $L_d = 37.5d$; $B = 5$	921 × 101
$L_u = 7.5d$; $L_d = 37.5d$; $B = 8$	921 × 161
$L_u = 7.5d$; $L_d = 37.5d$; $B = 10$	921 × 201
$L_u = 7.5d$; $L_d = 37.5d$; $B = 11$	921 × 221
$L_u = 7.5d$; $L_d = 37.5d$; $B = 12$	921 × 241
$L_u = 7.5d$; $L_d = 37.5d$; $B = 13$	921 × 261
$L_u = 7.5d$; $L_d = 37.5d$; $B = 14$	921 × 281
$L_u = 7.5d$; $L_d = 37.5d$; $B = 15$	921 × 301

VI. RESULTS AND DISCUSSIONS

Numerical calculations were carried out for flow around a square cylinder for upstream locations, downstream locations and blockages. The present calculations yield time series for the force coefficients, power spectra analysis of lift coefficient, and vorticity contours visualization and phase diagram for different combinations. Calculations of the mean drag coefficient, drag coefficient, Strouhal number, and root-mean-square values of drag and lift coefficients in terms of physical parameters for square cylinder are also given. It is important to mention here that we calculate the Strouhal number using the fast Fourier transform technique. In vorticity graphs the solid lines represent the positive vortices generated from the lower corner of the cylinder and dashed line presents the negative vortices generated from the upper corner. Moreover in drag coefficient, lift coefficient, Strouhal and phase graphs solid lines are used. In Tables exp. and num. means experimental and numerical, respectively. It is also important to mention here that in case of blockage we use the parabolic velocity profile at inlet instead of uniform inflow velocity. Furthermore, in this study we calculate the drag coefficient value by choosing the maximum value of the drag coefficient amplitudes. Those cases that they have similar characteristics are not shown in this paper and some representative cases will be discussed.

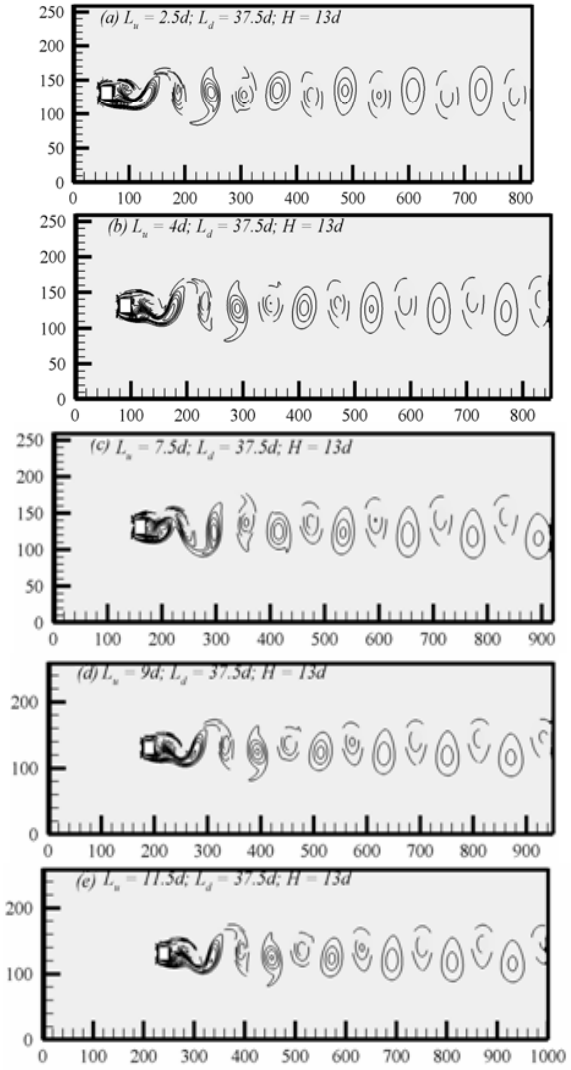

Fig. 3 Vorticity contour plot for $Re = 150$ at different upstream locations

A. Effect of Upstream Locations

To analyze the effect of upstream locations on vortex shedding, the vorticity contours are presented in Figs. 3 (a)-(e). From these figures, it can be easily observed that there is a significant change in the vortex shedding size and width behind the cylinder due to change in upstream location. The results show that the alternating vortices are shed from the upper and lower side of the cylinder for all chosen cases.

At $L_u = 2.5d$ and $4d$, a negative vortex on the upper side of the cylinder is roll up and at the same time on the lower side

of the cylinder a positive vortex appears. The vortex shedding process is almost similar to that shown for the case of L_u = 7.5d. Figs. 3 (d), (e) show that at L_u = 9d and 11.5d, a positive vortex on the lower side of the cylinder in the development process, while a negative vortex on the upper side of the cylinder is about to detach. The complete formation of positive and negative vortices observed for all cases with different width and size. The dynamics of the flow behind the cylinders and the observed changes in the vortex shedding pattern can also be easily observed with time change, power spectra analysis of lift coefficient and phase diagram from Figs. 4 (a)-(d), 5 (a)-(h), 6 (a)-(d), and 7 (a)-(d).

The time histories of drag and lift coefficients experienced by the cylinder are plotted in Figs. 4 (a)-(d) and 5 (a)-(h). When L_u = 2.5d, the drag (Fig. 4 (a)) and lift (Fig. 5 (a)) coefficients exhibit a regular behavior. This is actually related to the alternate vortex shedding observed behind the square cylinder. As L_u increase up to 11.5d the drag and lift coefficients magnitude decreases (Figs. 4 (b)-(d) and 5 (b)-(h)). As L_u increases, the amplitude of the lift coefficient decreases and as a result the width and size of the alternate shed vortices becomes stronger. At L_u = 2.5d and 4d, the shedding starts quickly as compared to other cases (Fig. 5 (a), (b)).

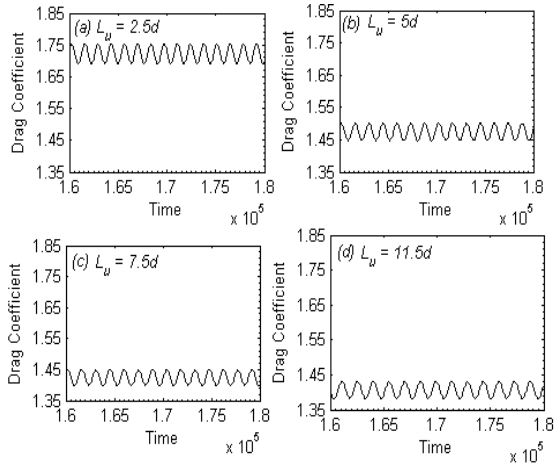

Fig. 4 Time-trace analysis of drag coefficient for Re = 150 at various upstream locations

The phase diagram and power spectra analysis of lift coefficient for different upstream locations are shown in Figs. 6 (a)-(d) and 7 (a)-(d), respectively. The eight type graphs observed for all chosen cases. This means that fully alternate vortex shedding generated behind the square cylinder. The drag and lift coefficients in phase diagram plots intersect each other at the mean position, which is the clear indication of symmetric vortices behind the square cylinder (Figs. 6 (a)-(d)).

The power spectrum analysis shows only one dominant peak for all chosen cases which is related to the vortex shedding behind the square cylinder.

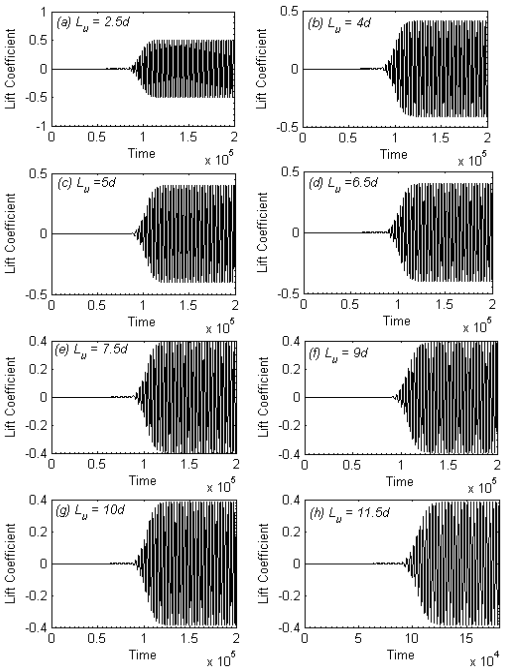

Fig. 5 Time-trace analysis of lift coefficient for Re = 150 at various upstream locations

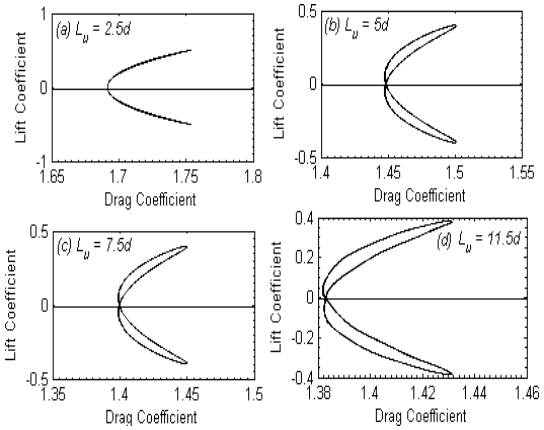

Fig. 6 Phase diagrams for various upstream locations at Re = 150

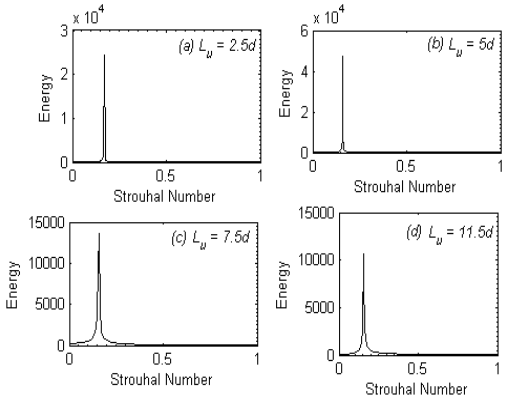

Fig. 7 Power spectra of lift coefficients at different upstream locations at Re = 150

TABLE II
COMPARISON OF PHYSICAL PARAMETERS FOR DIFFERENT UPSTREAM LOCATIONS

Cases	*Cdmean*	*Cd*	*St*	*Cdrms*	*Clrms*
Okajima [1] exp.		1.49	0.141		
Norberg [2] exp.			0.150		
Sohankar et al. [3] num.	1.408		0.161	0.0061	0.177
Saha et al. [4] num.		1.54	0.163		
Gera et al. [5] num.	1.411		0.141		0.252
$L_u = 2.5d$; $L_d = 37.5d$; $H = 13d$	1.722	1.75	0.164	0.0188	0.3050
$L_u = 4d$; $L_d = 37.5d$; $H = 13d$	1.524	1.55	0.1607	0.0196	0.2896
$L_u = 5d$; $L_d = 37.5d$; $H = 13d$	1.474	1.51	0.1580	0.0190	0.2742
$L_u = 6.5d$; $L_d = 37.5d$; $H = 13d$	1.437	1.46	0.1575	0.0184	0.2832
$L_u = 7.5d$; $L_d = 37.5d$; $H = 13d$	1.423	1.45	0.1547	0.0180	0.2805
$L_u = 9d$; $L_d = 37.5d$; $H = 13d$	1.413	1.44	0.1542	0.0176	0.2754
$L_u = 10d$; $L_d = 37.5d$; $H = 13d$	1.409	1.44	0.1547	0.0174	0.2725
$L_u = 11.5d$; $L_d = 37.5d$; $H = 13d$	1.405	1.44	0.1547	0.0174	0.2674

It is observed that the size of the computational domain have a great influence on the results for flow past bluff-body. It was found that the *Cdmean*, *Cd*, *St*, *Cdrms* and *Clrms* value decreased almost 17.3%, 17.2%, 6%, 4.3% and 8.1%, respectively, when increasing the upstream locations from $L_u = 2.5d$ to $7.5d$. Furthermore, it was found that by increasing the upstream location from $L_u = 7.5d$ to $11.5d$, the *Cdmean*, *Cd*, *St*, *Cdrms* and *Clrms* value decreased almost 1.3%, 0.7%, 0%, 3.3% and 4.7%, respectively. Sohankar et al. [3] observed 10% decreasing for upstream locations from smaller to the larger domain. On the basis of above analysis it was observed that the upstream location must be greater than or equal to $7.5d$. One can also choose $L_u = 6.5d$, because the influence of upstream location from $6.5d$ to $7.5d$ is almost negligible. In addition, we compare the result of $L_u = 7.5d$; $L_d = 37.5d$; $H = 13d$ with existing experimental data and numerical results. The results of *Cdmean*, *Cd*, *St*, *Cdrms* and *Clrms* are presented together with the experimental data of Okajima [1] and Norberg [2] in Table II. Some numerical results of Sohankar et al. [3], Saha et al. [4] and Gera et al. [5] are also presented in Table II for comparison. From the Table II, it can be clearly seen that the present numerical simulation results agree well with those in the literature. Moreover, it can also be found that the mean drag coefficient of present numerical result is closer to that of experimental data of Okajima [1] and numerical data of Gera et al. [5]. The Strouhal numbers obtained in the present work shows a good agreement with the experimental data of Norberg [2] and numerical data of Gera et al. [5]. In addition, also a good agreement observed for *Cdrms* and *Clrms* values.

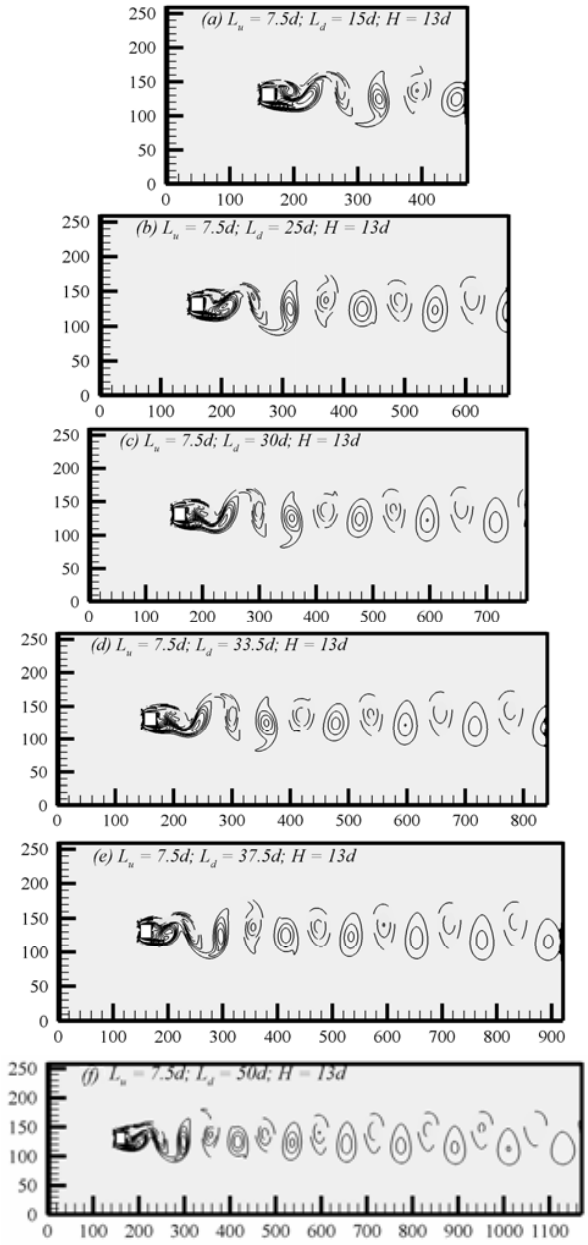

Fig. 8 Instantaneous vorticity contours visualization plot for $Re = 150$ at different downstream locations

B. Effect of Downstream Locations

The influence of the downstream location was studied separately for L_u = 7.5d and H = 13d. The effects of downstream locations on the flow structure behind the square cylinder are described in Figs. 8 (a)-(f). The results show that the alternating vortices are shed from the upper and lower side of the cylinder for all chosen cases. At L_d = 15d, a negative vortex on the upper side of the cylinder is roll up and at the same time on the lower side of the cylinder a positive vortex appears. The vortex shedding process is almost similar to that shown for the case of L_d = 25d. Figs. 8 (c), (d) show that at L_d = 30d and 33.5d, a positive vortex on the lower side of the cylinder is in the development process, while a negative vortex on the upper side of the cylinder is about to detach. The complete formation of positive and negative vortices observed for all cases with different width and size. At L_d = 37.5d, there are twelve vortices, six positive vortices and six negative vortices in the computational domain behind the square cylinder and the development process cut by the downstream location. In addition, the number of shed vortices increases for L_d = 50d (see Fig. 8 (f)).

The time histories of drag and lift coefficients experienced by the cylinder are plotted in Figs. 9 (a)-(d) and Figs. 10 (a)-(h). When L_d = 15d, the drag (Fig. 9 (a)) and lift (Fig. 10 (a)) coefficients exhibit a regular behavior. This is actually related the alternate vortex shedding observed behind the square cylinder. As L_d increases, the drag and lift coefficients magnitude almost becomes same.

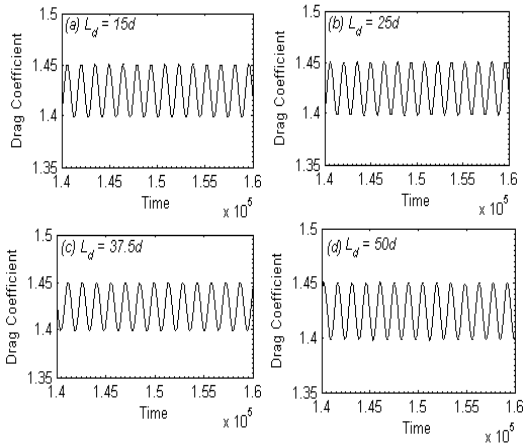

Fig. 9 Time-history analysis of drag coefficient for Re = 150 for various downstream locations

The time history analysis of drag and lift coefficient shows two crests and troughs, which ensures from the top and bottom surfaces the periodic vortex shedding. In addition, the formation of shedding occurs due to lift force fluctuation and therefore, its value of equal magnitude varies between a positive and negative maximum. One more interesting thing is observed that the computational time not affected too much by changing the downstream locations which is clearly observed from the lift coefficient plots (see Fig. 10 (a)-(h).

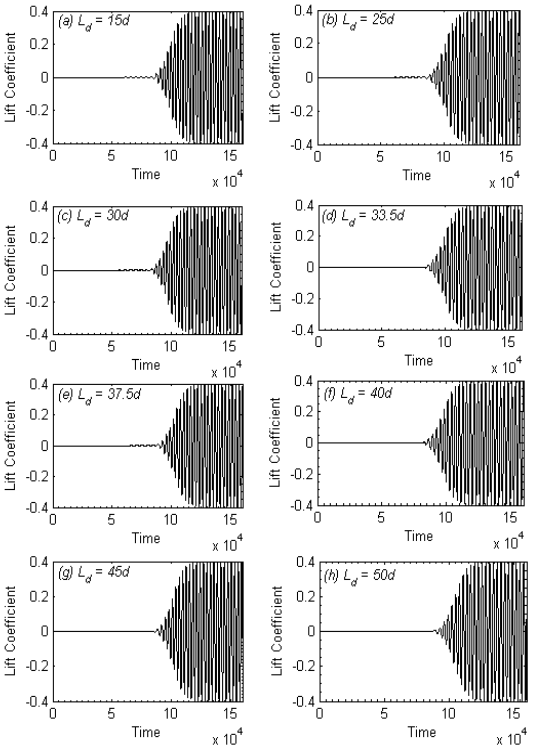

Fig. 10 Time-history analysis of lift coefficient for Re = 150 for various downstream locations

The phase diagram and power spectra analysis of lift coefficient are shown in Figs. 11-12 (a)-(d). It is clear from the graph that the alternate vortices generated behind the square cylinders for all chosen cases and the width and size of the vortices changes which clearly seen in phase diagram.

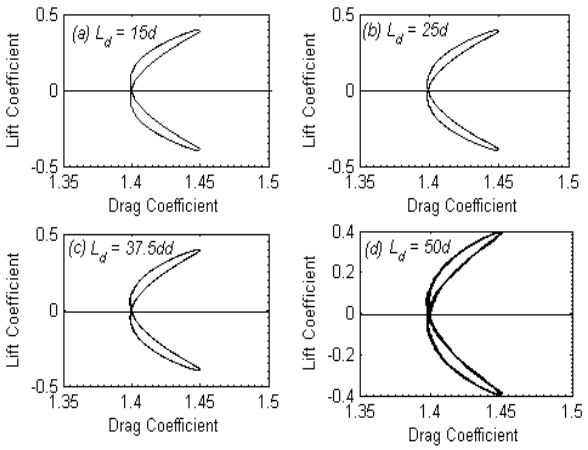

Fig. 11 Phase diagrams for different downstream locations at Re = 150

The poser spectrum analysis of lift coefficient reveals that the shed vortices travel downstream without any merging and distortion and as a result one can clearly see the single dominant peak in the spectrum analysis (Figs. 12 (a)-(d)).

Similar characteristics observed for L_d = 30d, 33.5d, 40d and 45d (not shown).

The results show that increasing the downstream location L_d = 15d to L_d = 37.5d the physical parameters such as mean drag coefficient, drag coefficient, Strouhal number, root-mean-square values of drag and lift coefficients decreased by 0.01%, 0.0%, 1.8%, 5.6%, and 6.5%, respectively (Table III). A further increase up to L_d = 50d gave almost negligible changes and almost less than 2%. Thus it is observed that L_d = 37.5d is an appropriate downstream location for flow past a single square cylinder. It is also suggested that dealing with complex flow past multiple bluff bodies one can choose L_d = 40d to 50d to provide more enough space for shed vortices behind the cylinders. Sohankar et al. [3] observed that L_d = 30d is appropriate downstream location and in some cases must be larger than this value.

TABLE III
COMPARISON OF PHYSICAL PARAMETERS FOR DIFFERENT DOWNSTREAM LOCATIONS

Cases	*Cdmean*	*Cd*	*St*	*Cdrms*	*Clrms*
Okajima [1] exp.		1.492	0.141		
Norberg [2] exp.			0.150		
Sohankar et al. [3] num.	1.408		0.161	0.0061	0.177
Saha et al. [4] num.		1.54	0.163		
Gera et al. [5] num.	1.411		0.141		0.252
L_u = 7.5d; L_d = 15d; H =13d	1.424	1.450	0.152	0.0170	0.262
L_u = 7.5d; L_d = 25d; H = 13d	1.424	1.450	0.1569	0.0170	0.262
L_u = 7.5d; L_d = 30d; H =13d	1.424	1.450	0.1578	0.01780	0.280
L_u =7.5d; L_d =33.5d; H=13d	1.4241	1.4502	0.1569	0.0181	0.279
L_u =7.5d; L_d =37.5d; H=13d	1.4239	1.450	0.1547	0.0180	0.280
L_u = 7.5d; L_d = 40d; H =13d	1.4241	1.4502	0.1578	0.0181	0.2809
L_u = 7.5d; L_d = 45d; H =13d	1.3909	1.450	0.1578	0.0301	0.2984
L_u = 7.5d; L_d = 50d; H =13d	1.3819	1.450	0.1578	0.0251	0.2495

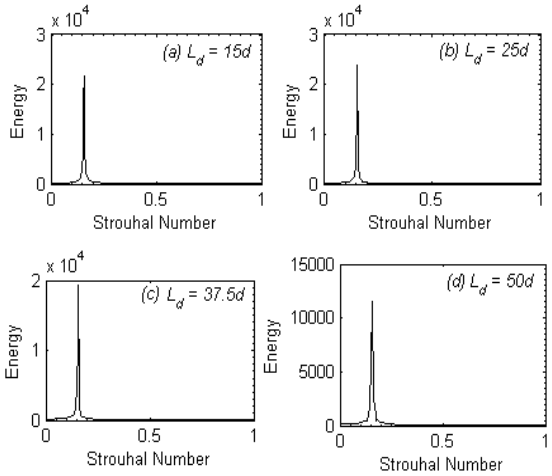

Fig. 12 Spectrum analysis of lift coefficients for different downstream locations at *Re* = 150

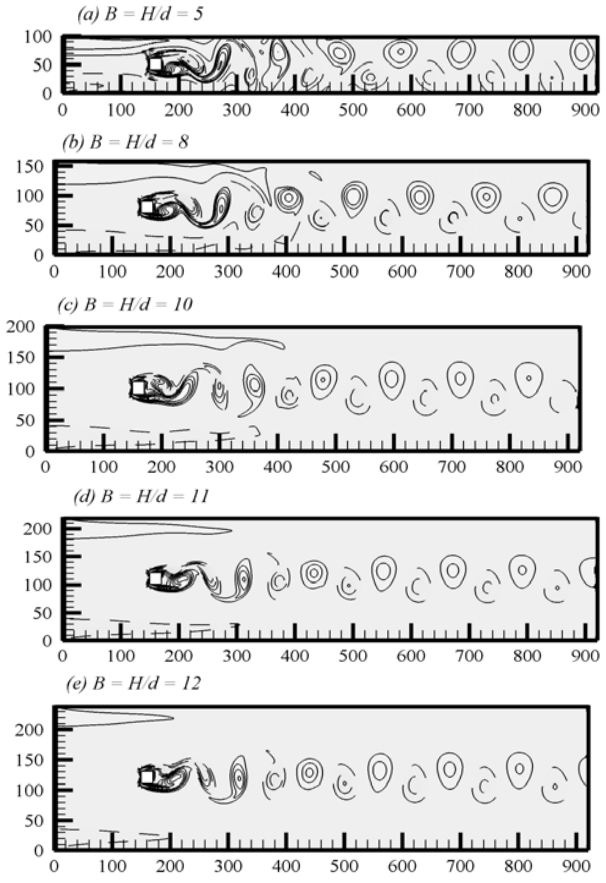

C. Blockage Effect

In this subsection we will discussed the channel height in other words the blockage effect for flow past a square cylinder. The vorticity contours visualization for different blockages are presented in Figs. 13 (a)-(h). At B = 5, the vortices shed behind the square cylinder and showing some distortion due to small spacing between the upper and lower walls of the channel (Fig. 13 (a)). As the value of B increases the effect of the blockage vanishes and the initial disturbance due to parabolic velocity profile are also vanish. The results show that $B \geq 12$, the wall effect almost negligible without affecting the shed vortices behind the square cylinder.

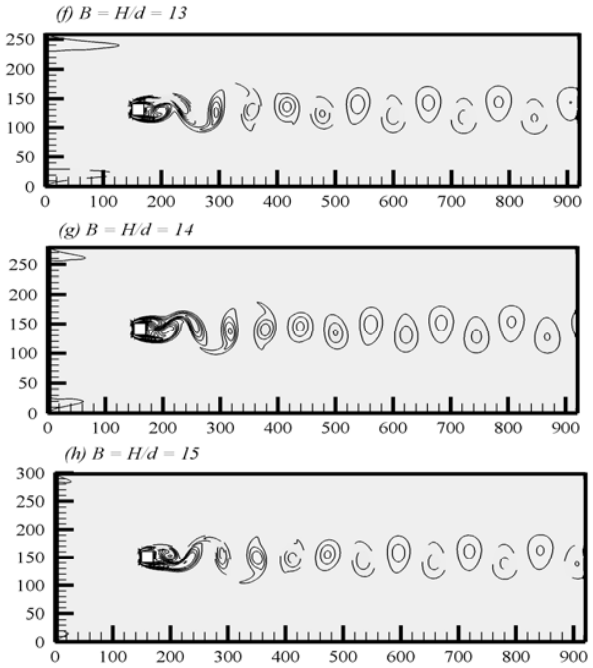

Fig. 13 Vorticity visualization plot for different blockages at *Re* = 150

The time-trace analysis of drag coefficient for some selected blockages is shown in Figs. 14 (a)-(d). It is observed that the magnitude of the drag coefficient increases when blockage increase. Moreover, the periodic variation observed for all chosen cases and some cases are not shown here.

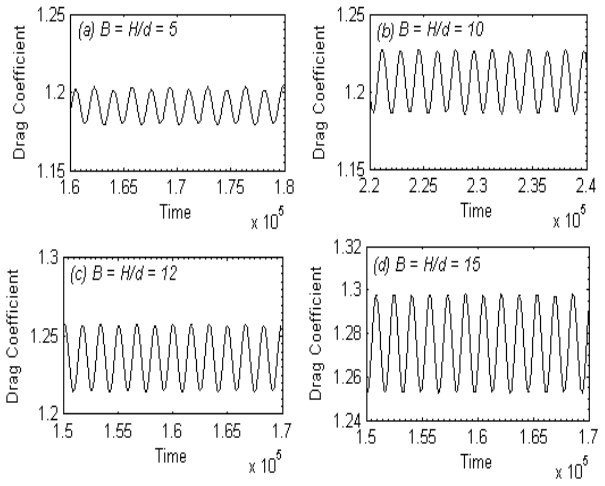

Fig. 14 Drag coefficient time-trace analysis at *Re* = 150 for various blockages

The time history analysis of lift coefficient for different blockages is shown in Figs. 15 (a)-(h). It is observed that the vortices shed almost at the same time for all chosen cases. The variation in amplitude is observed when the value of *B* increases.

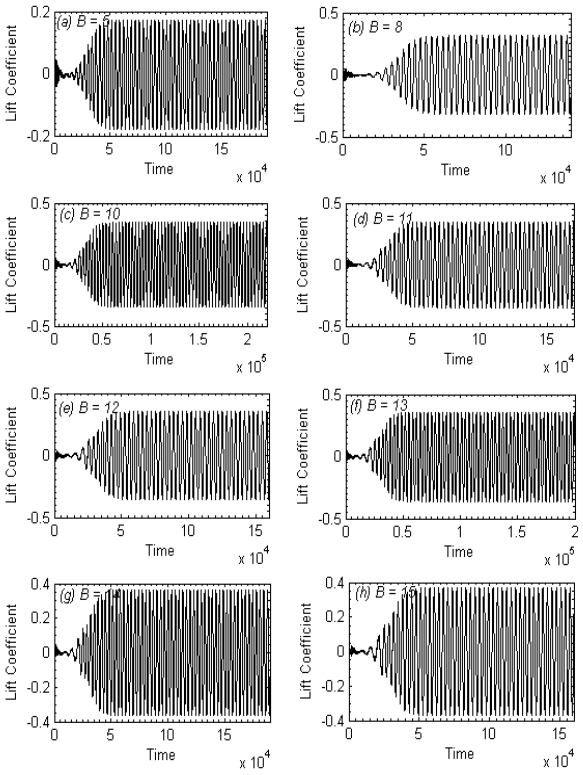

Fig. 15 Lift coefficient time-trace analysis at *Re* = 150 for various blockages

The phase diagram in Figs. 16 (a)-(d) shown that the alternate vortices generated behind the cylinder. Furthermore, the eight shape change because of different amplitude observed for different blockages.

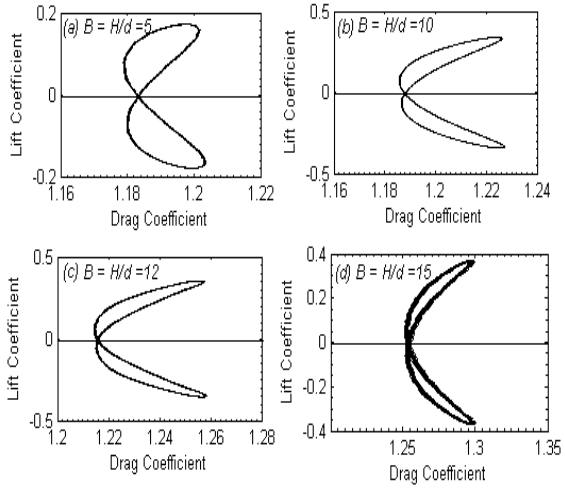

Fig. 16 Phase diagrams of drag and lift coefficients for different blockages at *Re* = 150

The power spectrum analysis of lift coefficient for some selected cases is shown in Figs. 17 (a)-(d). The amplitude of the spectrum increases with increasing blockage value, which

ensures the strength of the vortices behind the square cylinder. The single peak shows that there is no distortion of shed vortices behind the cylinder throughout the computational domain.

The physical parameters for different blockage values are shown in Table IV together with experimental data and numerical results for comparison. The decreasing behaviour observed for mean drag coefficient and drag coefficient from $B = 5$ to 8 and then show the increasing behaviour when the value of B increases. The similar trend was observed in the root-mean-square values of drag and lift coefficients. The blockage effect almost vanishes for $B \geq 12$.

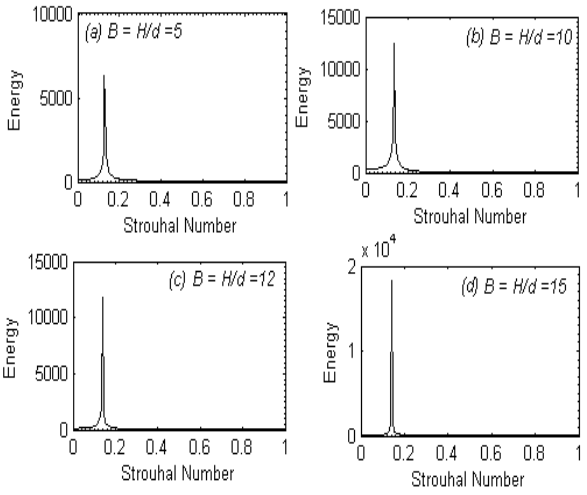

Fig. 17 Power spectra of lift coefficients for different blockages at $Re = 150$

TABLE IV
COMPARISON OF PHYSICAL PARAMETERS FOR DIFFERENT BLOCKAGES

Cases	*Cdmean*	*Cd*	*St*	*Cdrms*	*Clrms*
Okajima [1] exp.		1.492	0.141		
Norberg [2] exp.			0.150		
Sohankar et al. [3] num.	1.408		0.161	0.0061	0.177
Saha et al. [4] num.		1.54	0.163		
Gera et al. [5] num.	1.411		0.141		0.252
Lu =7.5*d*; *Ld* = 37.5*d*; *B* =5	1.190	1.215	0.131	0.0081	0.1241
Lu =7.5*d*; *Ld* = 37.5*d*; *B* =8	1.177	1.912	0.133	0.0155	0.2640
Lu=7.5*d*; *Ld* =37.5*d*; *B* =10	1.206	1.228	0.135	0.0142	0.2412
Lu=7.5*d*; *Ld* =37.5*d*; *B* =11	1.221	1.242	0.138	0.0151	0.2507
Lu=7.5*d*; *Ld* =37.5*d*; *B* =12	1.236	1.258	0.135	0.0151	0.2507
Lu=7.5*d*; *Ld* = 37.5*d*; *B* =13	1.250	1.272	0.141	0.0154	0.2544
Lu=7.5*d*; *Ld* =37.5*d*; *B* =14	1.263	1.282	0.143	0.0187	0.3070
Lu=7.5*d*; *Ld* =37.5*d*; *B* =15	1.275	1.295	0.141	0.0190	0.3110

VII. CONCLUSIONS

A numerical investigation of a uniform flow around a square cylinders with Reynolds number ($Re = 150$) for various upstream locations, downstream locations and blockages using the multi-relaxation-time lattice Boltzmann method has been studied. The effects in terms of time-trace analysis of drag and lift coefficients, power spectra of lift coefficient, phase diagram and the force statistics are examined in detail. From these results, distinctive flow differences and sensitivity on the physical parameters are summarized as follows:

(i) It is found that the upstream location have a great influence on the results for flow past bluff-body. It is observed that the *Cdmean*, *Cd*, *St*, *Cdrms* and *Clrms* value decreased almost 17.3%, 17.2%, 6%, 4.3% and 8.1%, respectively, by increasing the upstream locations from $L_u = 2.5d$ to $7.5d$. Furthermore, by increasing the upstream location from $L_u = 7.5d$ to $11.5d$, the *Cdmean*, *Cd*, *St*, *Cdrms* and *Clrms* value decreased almost 1.3%, 0.7%, 0%, 3.3% and 4.7%, respectively. The size and width of the shed vortices also affected for different upstream locations.

(ii) The results show that by increasing the downstream location $L_d = 15d$ to $L_d = 37.5d$ the physical parameters such as mean drag coefficient, drag coefficient, Strouhal number, root-mean-square values of drag and lift coefficients decreased by 0.01%, 0.0%, 1.8%, 5.6%, and 6.5%, respectively. A further increase up to $L_d = 50d$ gave almost negligible changes and almost less than 2%. Thus it is observed that $L_d = 37.5d$ is an appropriate downstream location for flow past a single square cylinder.

(iii) It is found that the height of the computational domain must be $H = 12d$ for good results. At this value the shed vortices and physical parameters are not affected too much.

REFERENCES

[1] A. Okajima, "Strouhal numbers of rectangular cylinders," *Journal of Fluid Mechanics*, vol. ED-123, pp. 379-398, 1982.W.-K. Chen, *Linear Networks and Systems* (Book style). Belmont, CA: Wadsworth, pp. 123–135, 1993.

[2] C. Norberg, "Flow around rectangular cylinders: Pressure forces and wake frequencies," *Journal of Wind Engineering and Industrial Aerodynamics*, vol. ED-40, pp. 187-196, 1993.

[3] A. Sohankar, L. Davidson, and C. Norberg, "Numerical simulation of unsteady flow around a square two-dimensional cylinder," *The Twelfth Australian Fluid Mechanics Conference, The University of Sydney, Australia*, pp. 517-520, 1995.
[4] A. K. Saha, G. Biswas, and K. Muralidhar, "Three-dimensional study of flow past a square cylinder at low Reynolds numbers," *International Journal of Heat and Fluid Flow*, vol. ED-24, pp. 54-66, 2003.
[5] B. Gera, P. K. Sharma, and R. K. Singh, "CFD analysis of 2D unsteady flow around a square cylinder," *International Journal of Applied Engineering Research, Dindigul*, vol. ED-1, pp. 602-610, 2010.
[6] S. Ul. Islam, and C. Y. Zhou, "Characteristics of flow past a square cylinder using the Lattice Boltzmann method," *Information Technology Journal,* vol. ED-8, pp. 1094-1114, 2009.
[7] K. Suzuki, and K. Inaoka, "Flow modification and heat transfer enhancement with vortices," *International Journal of Transport Phenomena*, vol. ED-1, pp. 17-30, 1998.
[8] A. Sohankar, C. Norberg, and L. Davidson, " Low-Reynold flow around a square cylinder at incidence: study of blockage, onset of vortex shedding and outlet boundary condition," *International Journal of Numerical Methods in Fluids*, vol. ED-26, pp. 39-56, 1998.
[9] M. S. M. Ali, C. J. Doolan, and V. Wheatley, " Grid convergence study for a two-dimensional simulation of flow around a square cylinder at a low Reynolds number," *Seventh International Conference on CFD in the Minerals and Process Industries CSIRO, Melbourne, Australia, 9-11 December*, pp. 1-6*, 2009*.
[10] X. Ying, F. Xu, and Z. Zhang, " Numerical simulation and visualization of flow around rectangular bluff bodies," *The Seventh International Colloquium on Bluff Body Aerodynamics and Applications (BBAA7) Shanghai, China, September* 2-6, 2012, pp. 272-281.
[11] C. J. Doolan, "Flat-plate interaction with the near wake of a square cylinder," *AIAA Journal*, vol. ED-47, pp. 475-478, 2009.
[12] U. Frisch, D. Hasslacher, and Y. Pomeau, "Lattice-gas automata for the Navier-Stokes equation," *Physical Review Letters*, vol. ED-56, pp. 1505-1508, 1986.
[13] P. L. Bhantnagar, E. P. Gross, and M. A. Krook, "A model for collision processes in gases. I. Small amplitude processes in charged and neutral one-component systems," *Physical Review Letters*, vol. ED-94, pp.511-525, 1954.
[14] P. Lallemand and L. S. Luo, "Theory of the lattice Boltzmann method: dispersion, dissipation, isotropy, Galilean invariance, and stability," *Physical Review Letters E*, vol. ED-61, pp.6546-6562, 2000.
[15] I. Ginzburg, and D. d'Humieres, "Multireflection boundary conditions for lattice Boltzmann models," *Physical Review E*, vol. ED-68, pp.066614, 2003.
[16] D. d'Humieres, "Generalized lattice Boltzmann equations. In Rarefied Gas Dynamics: Theory and Simulations," Shizgal BD, Weaver DP (eds). Progress in Astronautics and Aeronautics. Vol. 159. AIAA Press: Washington, DC, pp. 450-458, 1992.
[17] S. Ul. Islam, and C. Y. Zhou, "Numerical simulation of flow around a row of circular cylinders using the Lattice Boltzmann method," *Information Technology Journal*, vol. ED-8, pp.513-520, 2009.
[18] M. Cheng, D. S. Whyte, and J. Lou, "Numerical simulation of flow around a square cylinder in uniform shear flow," *Journal of Fluids and Structures*, vol. ED-23, pp. 207-226, 2007.
[19] W. S. Abbasi, S. Ul. Islam, S. C. Saha, Y. T. Gu, and C. Y. Zhou, "Effect of Reynolds numbers on flow past four square cylinders in an in-line square configuration for different gap spacings," *Journal of Mechanical Science and Technology*, vol. ED-28, pp. 539-552, 2014.
[20] Z. Guo, H. Liu, LI-S. Luo, and K. Xu, "A comparative study of the LBE and GKS methods for 2D near incompressible laminar flows," *Journal of Computational Physics*, vol. ED-227, pp. 4955-4976, 2008.
[21] S. Ul. Islam, C. Y. Zhou, and F. Ahmad, "Numerical simulations of cross-flow around four square cylinders in an in-line rectangular configuration," *World Academy of Sciences, Engineering and Technology*, vol. ED-3, 2009.
[22] C. Rettinger, "Fluid flow simulations using the lattice Boltzmann method with multiple relaxation times, Friedrich-Alexander-Universitat Erlangen-Nurnberg, Technische Fakultat. Department Informatik, Bachelor Thesis, 2013.
[23] S. Ul. Islam, C. Y. Zhou, A. Shah, and P. Xie, "Numerical simulation of flow past rectangular cylinders with different aspect ratios using the incompressible lattice Boltzmann method," *Journal of Mechanical Science and Technology*, vol. ED-26, pp. 1027-1041, 2012.
[24] A. R. Rahmati, M. Ashrafizaadeh, and E. Shirani, "A multi-relaxation-time Lattice Boltzmann method on non-uniform grids for large eddy simulation of Rayleigh-Benard convection using two sub-grid scale models," *Journal of Applied Fluid Mechanics*, vol. ED-7, pp. 89-102, 2014.
[25] D. P. Ziegler, "Boundary conditions for lattice Boltzmann simulations," *Journal of Statistical Physics*, vol. ED-71, pp.1171-1177, 1993.
[26] Y. Dazchi, M. Renwei, L. S. Luo, and S. Wei, "Viscous flow computations with the method of lattice Boltzmann equation," *Progress in Aerospace Sciences*, vol. ED-39, pp. 329-367, 2003.